Formation and decay of the composite system in ^{40}Ar-induced reactions at 15 MeV/nucleon

D. Pelte, U. Winkler, M. Bühler, and B. Weissmann
Physikalisches Institut der Universität Heidelberg, D-6900 Heidelberg, Federal Republic of Germany and Max-Planck-Institut für Kernphysik, D-6900 Heidelberg, Federal Republic of Germany

A. Gobbi, K. D. Hildenbrand, and H. Stelzer
Gesellschaft für Schwerionenforschung (GSI), D-6100 Darmstadt, Federal Republic of Germany

R. Novotny
II. Physikalisches Institut der Universität Giessen, D-6300 Giessen, Federal Republic of Germany
(Received 17 January 1986)

The reactions ^{40}Ar+^{27}Al, ^{45}Sc, ^{58}Ni, ^{90}Zr are studied at 600 MeV bombarding energy. The experiments employ several large-area detectors of different kinds to identify heavy fragments and measure their multiplicity. Two- and three-fragment channels are observed in all reactions and their cross sections are determined. The existence of four-fragment channels is suggested by the experiment; their contribution is, however, too weak for a detailed analysis. In addition to the multifragmentation processes, the emission of light particles is also observed, the average charge of all emitted particles being slightly smaller than expected from experiments at lower energies. The predominant source of light particles is the evaporation from hot fragments. In the light systems the existence of three fragments is ascribed to a fast disintegration process, whereas in the heaviest system a major part of such channels could also arise from a sequential fission process.

I. INTRODUCTION

Heavy-ion reactions become increasingly more complex with increasing bombarding energy. New phenomena occur at energies between 10 and 100 MeV/u. These are, e.g., the incomplete momentum transfer (for a recent example, see Ref. 1) or the production of several fragments, may it be either by evaporation[2–5] or fast multifragmentation.[6–9] The incomplete momentum transfer, which can be observed in the experiments described herein, will be discussed in a forthcoming paper. The present paper is solely concerned with the possible mechanisms of fragment production. The evaporation of complex particles has been previously observed in light-ion ($M \leq 14$) induced reactions.[2–5] Although the results have been mainly interpreted in terms of a nuclear temperature of the evaporating system,[4,10–13] other mechanisms predict almost identical results[14–16] and thus the true nature of the "evaporation" process should be considered still unclear. Multifragmentation has been observed in reactions with heavier projectiles and targets. At energies around 10 MeV/u the fission of one or both fragments after a normal deep-inelastic reaction appears to be the dominant mechanism.[6,9] At higher energies, however, the separation into two or more successive processes becomes more and more artificial.[7,8] Indeed, theory predicts prompt multifragmentation to occur at sufficiently high nuclear temperatures.[17,18] Furthermore, one may expect that nuclear systems before breakup pass through novel configurations because of the high temperatures and angular momenta involved.[19] The experimental identification of these phenomena and their clear separation are difficult problems. One of the simpler means appears to rely on the spectrum of produced elements. In the case in which the production is of evaporative nature and is thus fundamentally not different from the evaporation process that leads to the emission of light particles, the work of, e.g, Sobotka *et al.*[4] has demonstrated that the production cross section rapidly decreases with increasing atomic number. If expressed in terms of a power law $d\sigma/dZ=\sigma_0 Z^{-\tau}$, the production cross section may be characterized by a representative value of $\tau \approx 3$. On the other hand, recent statistical treatments of the multifragmentation process in Refs. 17 and 18 resulted in element distributions at threshold energies which are much less steeply dependent upon fragment charge. These results are more comparable to a power law expression with a smaller exponent of $\tau \geqq 1$. Of similar importance certainly are the associated particle and fragment multiplicities, about which, however, almost nothing is experimentally known.

The experimental investigations described in this paper are performed at an energy of 15 MeV/u. This energy is still close to the upper limit where heavy-ion reactions show the normal low-energy behavior,[20,21] but high enough that novel features become clearly observable. Most striking is the sudden increase in the width of the distribution of elements produced in deep-inelastic reactions.[21] In the case of ^{92}Mo + ^{92}Mo reaction this increase was successfully described by a change from a single-nucleon exchange mechanism to a collective mechanism where the properties of the exit channel are determined by the bulk properties (temperature, nuclear densities, etc.) of the nuclear systems involved. In addition, and with contributions of 10–30% to the binary deep-inelastic process, the fragmentation into at least three heavy nuclei has

been identified in this energy range.[7–9,21] This process has been observed in light-, medium-, and heavy-ion reactions; its strength appears to depend strongly on the bombarding energy. In the case of heavy ions a detailed analysis of the experimental results[7] suggests that the disintegration is complete before the fragments have left their mutual interaction volume. This view is still controversial for medium ion systems;[9] in the case of very light ions, however, the results are best understood by assuming a fast disintegration process.[8]

With the present investigations we have continued our studies[8,22,23] of medium heavy-ion reactions using ^{40}Ar projectiles and ^{27}Al, ^{45}Sc, ^{58}Ni, and ^{90}Zr targets. The experimental techniques used are very similar to those used in the previous experiments. The reader is referred to these publications in the cases where specific points are not fully discussed in the present paper. In short, our technique consists of measuring all kinematic quantities of fragments with atomic number $Z \geq 4$ and reconstruction of the properties of light ($Z < 4$) particle emission using the conservation laws. In this way it was learned earlier, for example, that the total nuclear charge of all evaporated particles increases linearly with the c.m. energy and thus is a good measure for the inelasticity of the reaction.[22] Usually the measured fragment multiplicities were $m_f = 2$; with much less probability, $m_f = 3$ events were also observed. The reduction is not only due to the smaller cross section for the latter events, but also depends critically on the detectors and their geometric configuration. In Sec. II we give the details of the detectors employed and of the geometric setup, and discuss to some extent the problems of the kinematic analysis, particularly the deduction of absolute cross sections. Section III contains the experimental results, which are ordered according to the measured fragment multiplicity. In the discussion, Sec. IV, we compare our results to other relevant data and elaborate on the experimental evidence for the formation of an intermediate system that has oblate shape and high angular momentum. The summary of the present investigations is contained in Sec. V.

II. EXPERIMENTAL TECHNIQUES

A. Experimental setup

The ^{40}Ar beam was supplied by the UNILAC accelerator of the Gesellschaft für Schwerionenforschung (GSI), Darmstadt. The beam energy was 600 MeV and the accelerator operated at a frequency of 27 MHz with a beam-pulse resolution of 300 ps at the target position. Four different targets were used and their thicknesses are given in parantheses as follows: ^{27}Al (558 μg/cm^2), ^{45}Sc (368 μg/cm^2), ^{58}Ni (586 μg/cm^2), and ^{90}Zr (51 μg/cm^2). All targets were isotopically enriched and self-supporting foils, except for the ^{90}Zr target, which was evaporated onto a 5 μg/cm^2 thick carbon foil. The target thicknesses were determined by energy loss measurements of alpha particles. The contamination of the targets with other elements was checked by methods that were previously described.[23] The targets were found uncontaminated, except for the ^{90}Zr target, which had, as expected, a considerable contamination from carbon and oxygen isotopes.

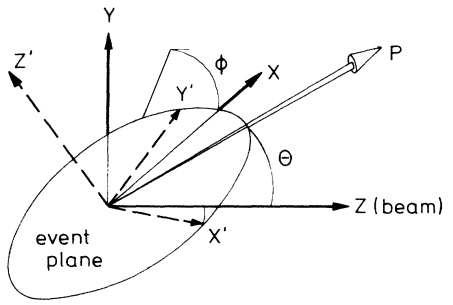

FIG. 1. Schematic view of the Cartesian coordinates of event P in the laboratory frame x,y,z. Also shown is the event plane with coordinate frame x',y',z' which moves relative to the laboratory frame with velocity $v_{\text{c.m.}}$. $v_{\text{c.m.}} = 0$ is assumed.

Reaction products with atomic numbers $Z \geq 4$ were detected by three large ionization chambers, each of which had a double detection capability. The peformance of this detector type and its geometric proportions were described in Ref. 8 in detail. We do not repeat this description here, but use the identical nomenclature. A schematic picture of the coordinate frames used most often to describe the detector settings and the data is presented in Fig. 1. The symmetry axis of the detector on the right-hand side of the beam could be positioned at angles $\theta_{\text{III}} = 26.5°, 40°, 70°$. The symmetry axes of the two detectors on the left-hand side of the beam could be positioned at $\theta_{\text{I}} = 47.8°, 62.8°, 77.8°$ and $\theta_{\text{II}} = 16.2°, 31.2°, 46.2°$. In total, a maximum of nine different detector settings were selected in the run with the ^{58}Ni target. In other runs the number of detector settings was smaller because of the different kinematic situations.

In addition to the ionization chambers two parallel-plate avalanche detectors were employed.[24] They were positioned at $\theta_A = 29°, \phi_A = 121°$ and $\theta_B = 28°, \phi_B = 242°$, and each covered a solid angle of $d\Omega = 323$ msr. The kinematic quantities measured by these detectors are the time of flight and the recoil direction of the nucleus being detected. These three quantities are not sufficient to be incorporated into the kinematic analysis described in the next subsection. Therefore the data were used to confirm the results from this analysis. For example, the recoil direction of the deficit (cf. subsection B) was compared to the impact location in the parallel-plate detectors. Of particular importance is the fact that the detection efficiency of these detectors rapidly decreases for Z values below $Z = 6$, where the detection efficiency is about 60%. This allows one to select fragment-fragment coincidences between the ionization chambers and the parallel-plate detectors.

The fragment energies measured by the ionization chambers were corrected for energy losses in the target and the entrance foil of the detector. Depending on the gas pressure, this detector type has a lower and upper limit of energies between which the fragment's nuclear charge can be identified. If the energy is too small, the fragments do not produce a sufficiently long ionization track in the chamber; in the other case they are not com-

pletely stopped. The lower and upper energy limits under the present conditions are $E_{\min}=3.47Z$ and $E_{\max}=22.22Z$, where energies are given in MeV and charges in units of e. The lower limit allows one to measure reactions of maximum energy loss (cf. Sec. III); the upper limit, however, is too small to register all reactions with very small energy losses. The situation could be improved by increasing the gas pressure with the result of less efficiency for strongly damped collisions. We have decided that the latter, for the intentions of the present investigations, should have a large detection efficiency.

B. Kinematic analysis

The principles of the kinematic analysis have been described in previous papers.[8,22] Using the kinematic quantities Z_i, $\mathbf{p}_i$, and E_i of all m_f fragments detected by the ionization chambers, one solves the equations

$$\begin{aligned} Z_0&=\sum Z_i+\Delta Z \quad (1\leqq i\leqq m_f)\ , \\ M_0&=\sum M_i+\Delta M\ , \\ \mathbf{p}_0&=\sum \mathbf{p}_i+\Delta \mathbf{p}\ , \\ E_0&=\sum E_i+\Delta E-Q \end{aligned} \tag{1}$$

to obtain the corresponding deficit quantities characterized by the front letter Δ. The index 0 refers to the entrance channel. The equation with respect to the nuclear masses is included for reasons of completeness. In the analysis the mass for a given nuclear charge is taken to be that with the largest abundance in the valley of nuclear stability (cf. Ref. 23). The deficits combine the contributions from all particles not detected. For the normal evaporation these will be predominantly light particles with charge $Z\leqq 2$ and mass $M\leqq 4$. Obviously, the last equation in set (1) cannot be conclusively solved for both ΔE and Q. It is thus impossible to obtain the kinetic energy loss $|Q|$ without correcting the measured energies to account for the evaporation. An approximate evaporation correction may be performed with the assumption that the charge evaporated from a nucleus is proportional to the charge of that nucleus. This assumption is based on an average energy sharing between the fragments that is proportional to their charge. One then obtains

$$\begin{aligned} Z_i^{\rm corr}&=(1+\alpha)Z_i\ , \\ \mathbf{p}_i^{\rm corr}&=(1+\alpha)(\mathbf{p}_i+\delta\mathbf{p}_i)\ , \end{aligned}$$

where $\alpha=\Delta Z/(Z_0-\Delta Z)$. The corrected masses $M_i^{\rm corr}$ are assumed to be related to the corrected nuclear charges in the same way that was stated above. The corrections $\delta\mathbf{p}_i$ only vanish when the velocity of the nucleus is not changed by the evaporation. This, however, is true only on the average. In the event-by-event correction, it is required that the momentum deficit after the corrections becomes zero. This can be accomplished by

$$\delta\mathbf{p}_i=[(1+\alpha)\Delta\mathbf{p}-\alpha\mathbf{p}_0]M_i/M_0\ .$$

The formula is derived with the assumption that for each event the change of the velocity is the same for all fragments produced. Using the corrected masses and momenta the corrected energies and Q values are

$$E_i^{\rm corr}=(p_i^{\rm corr})^2/2M_i^{\rm corr},\quad Q^{\rm corr}=\sum E_i^{\rm corr}-E_0\ .$$

Because of the various assumptions that enter the corrections, it is estimated that the mean values of Q are correct within $\pm 10\%$. The uncertainty is larger ($\delta Q=\pm 50$ MeV) when Q is calculated on the event-by-event basis. We thus do not think it useful to present the data as functions of the Q value.

The conservation of linear momentum, the third equation of set (1), implies that for $m_f=2$ the three momenta $\mathbf{p}_1'$, $\mathbf{p}_2'$, and $\Delta\mathbf{p}'$ in the center-of-mass system define a plane which is called the event plane. The orientation of this plane with respect to the beam axis is obtained by diagonalizing the momentum tensor,

$$\mathscr{P}'_{\alpha,\beta}=\sum p'_{\alpha,i}p'_{\beta,i}\ ,$$

where α,β refer to the Cartesian coordinates x,y,z of the momenta and the summation includes the momentum deficit. With the three eigenvalues and eigenvectors $\mathscr{P}'_k,\hat{\mathbf{e}}'_k$, ordered with respect to their magnitudes, $\mathscr{P}'_1\geqq\mathscr{P}'_2\geqq\mathscr{P}'_3$, the orientation may be represented by the quantity $\cos\alpha=\hat{\mathbf{e}}'_3\mathbf{p}'_0/p'_0$. In general, $\cos\alpha$ has a distribution which is symmetric around $\cos\alpha=0$. Thus one always has $\langle\cos\alpha\rangle=0$ regardless of the orientation of the event plane. When the mean value of the event-plane orientation is required, the better quantity is the second moment $\langle\cos^2\alpha\rangle$. One has $\langle\cos^2\alpha\rangle=0$ when the normal of the event plane is perpendicular to the beam momentum and $\langle\cos^2\alpha\rangle=1$ when it is parallel to the beam momentum. In the case in which the number of fragments is $m_f>2$, the event plane and its orientation can be still defined in this way. However, the momenta are not necessarily in this plane. The amount by which the momenta are out of a truly plane configuration may be obtained by using the eigenvalues $\mathscr{P}'_k$ and defining the planarity $\cos\delta=\mathscr{P}'_3/\mathscr{P}'$, where $\mathscr{P}'=(\mathscr{P}'^2_1+\mathscr{P}'^2_2+\mathscr{P}'^2_3)^{1/2}$. In the case in which all momenta are in the event plane, one has $\cos\delta=0$; otherwise, $0<\cos\delta\leqq 0.577$. For a random distribution, $\langle\cos\delta\rangle=0.247$.

In Fig. 1 we display the two coordinate frames used in the analysis. The Cartesian coordinates x,y,z define the laboratory system, with z having the direction of the beam momentum, and θ,ϕ are the usual polar angles in the frame. The c.m. system is given by the Cartesian coordinates x',y',z', where z' is the normal vector onto the event plane and x' is given by projecting the beam momentum into the event plane.

In experiments like ours, where the detectors do not have 4π geometry, the experimental results depend on the imposed phase-space restrictions. The influence of such restrictions has to be studied by Monte Carlo simulations. It is fairly easy to implement the detector geometries and efficiencies into the simulations. More cumbersome is the choice of the correct event generator, which should produce sample distributions similar to those produced by the reaction. Here one has to find a compromise between the complexity of the reaction and the time required for

Monte Carlo simulations. With respect to the emission process of particles and fragments, we have assumed that both are simultaneously emitted. Although this is most likely incorrect for the particle emission, the great number of them ensures that this assumption has no severe effect on the distributions of the fragments that are the only ones detected. The directional and momentum distributions of particles and fragments in the c.m. system were assumed to be random. The momenta depend on the available energy E. This parameter E was assumed to vary between $V_C < E < E'_0 + Q_g$, where V_C and E'_0 are the Coulomb-barrier height and c.m. kinetic energy of the entrance channel, and Q_g is the ground-state mass defect of a specific exit channel. In general, 30 different exit channels were included in one simulation; they were selected to reproduce the previously observed broad element distributions[21] and the measured charge-deficit distribution. Since the Q_g value becomes increasingly more negative with the number of emitted particles and the mass asymmetry of the fragments, this procedure favors reactions with large kinetic energy loss. This is in accordance with the observation that a major part of the reaction cross section is exhausted by deep-inelastic processes.[25] The data generated by the Monte Carlo simulations are used for two purposes: On one hand, a comparison between the experimental data and the Monte Carlo data indicates strong deviations from the assumption on which the event generator is based. Such deviations are observed, for example, in the properties of the event plane. On the other hand, the Monte Carlo simulations allow one to determine the detection efficiencies. For reactions with a given detector setting and with two fragments in the exit channels, both being detected, the efficiencies are of the order of $\epsilon \approx 8 \times 10^{-3}$. The corresponding case with three fragments emitted and three detected has an efficiency $\epsilon \approx 5 \times 10^{-4}$. It must be realized that these values for the total efficiencies depend on the specific properties of the event generator. By comparing the results from the different detector positions, it is concluded that the ϵ are uncertain to at least $\pm 25\%$. Cross sections cannot be deduced from this experiment with higher accuracy; however, the relative strength of cross sections can be trusted to have a smaller uncertainty.

III. EXPERIMENTAL RESULTS

The experimental results are presented according to the measured fragment multiplicities $m_f = 1,2,3$. Note that the value of m_f does not necessarily give the correct number of fragments produced by the reaction. The value of m_f is also determined by the reaction kinematic on one hand and by the detector setup on the other. However, for a given value of m_f, the correct number of fragments has to be equal or larger than m_f. These two possibilities can often be distinguished in the data because the amount of measured quantities exceeds the minimum amount necessary for an exclusive analysis. In the presentation of the data we will switch between the different targets at random, when the corresponding data show a similar behavior. When they are different, results for each target will be presented.

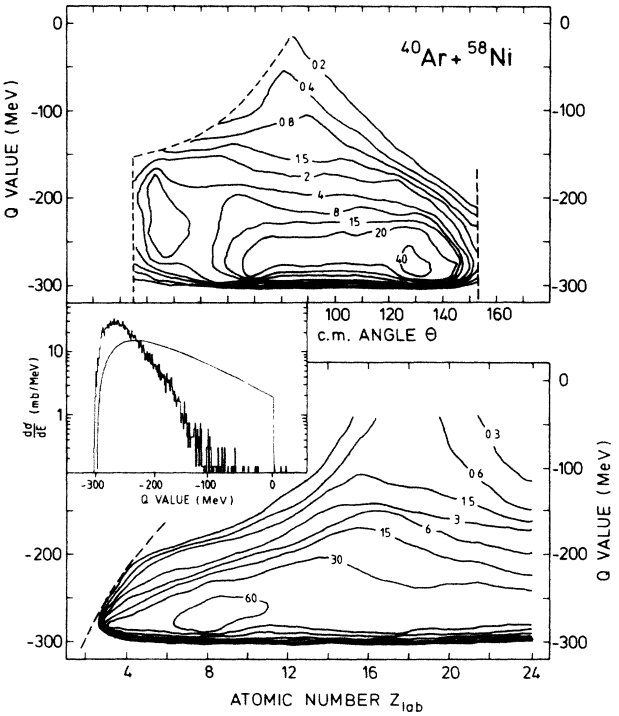

FIG. 2. Contour plots of the Q value vs the c.m. angle of the light fragment [above, the numbers give the cross section in mb/(5° MeV)] and the atomic number of the light fragment [below, the numbers give the cross section in mb/(e MeV)]. The dashed curves represent the efficiency cuts due to the detector properties; the inset compares the measured Q-value distribution with the prediction of Refs. 25 and 26.

A. The $m_f = 1$ events

The data with fragment multiplicity $m_f = 1$ were treated as binary reactions since the detection of evaporation residues is not possible at the chosen detector angles. However, the assumption of a true binary reaction is incorrect also since we shall prove in the next subsection that light-particle evaporation, after the binary reaction, is the most probable process. Nevertheless, with the binary analysis it is possible to give a rough overview of the reactions under the prevailing conditions and to compare the results to those from other studies which are based on a similar analysis.

In Fig. 2 we display the Q-value spectrum $d\sigma/dQ$ of the $^{40}\mathrm{Ar} + {}^{58}\mathrm{Ni}$ reaction and the two dimensional plots $d\sigma/dZ$ vs $d\sigma/dQ$ and $d\sigma/d\theta_{\mathrm{c.m.}}$ vs $d\sigma/dQ$. These diagrams include data from all detector positions. The dotted curves represent the absolute detection boundaries of the experimental arrangement due to the energy cutoffs at small and large energies and due to the positions of the detectors and their solid angles. Note that the grazing angle for the $^{40}\mathrm{Ar} + {}^{58}\mathrm{Ni}$ reaction at 600 MeV bombarding energy is estimated to be 14° in the c.m. system. The integrated cross section of this reaction is deduced to be $\sigma_{\mathrm{tot}} = 1927$ mb. This value is the measured cross section corrected for the detection efficiencies in a way that was described earlier. The predicted value[25,26] of the integrated cross section is $\sigma_{\mathrm{tot}} = 2370$ mb. The corresponding re-

TABLE I. Predicted and measured cross section for the reactions $^{40}Ar + {}^{27}Ar$, ^{45}S, ^{58}Ni, ^{90}Zr. From the cross sections, upper values of the angular momenta are deduced using the sharp cutoff model.

Atomic mass	Prediction σ_{fus} (mb)	Prediction l_{cr} ($\hbar$)	Prediction σ_{tot} (mb)[a]	Measurement σ_{tot} (mb)	Measurement l_{max} ($\hbar$)	Measurement $\sigma_{tot}(2)$ (mb)	Measurement $\sigma_{tot}(3)$ (mb)
67	501	54	2024	811±240	88 ±8	711±210	100± 30
85	485	70	2305	1176±360	130±14	1032±310	144± 50
98	506	80	2375	1927±580	176±21	1494±450	433±130
130	521	95	2569	2572±800	232±30	2404±720	168± 80

[a] $\sigma_{tot}=0.9\,(\sigma_{reac}-\sigma_{fus})$; cf. Refs. 25 and 26.

sults and predictions for the other targets are listed in Table I. The table also includes the predictions for the fusion component of the reactions. In order to obtain a feeling for the effect which the strong evaporation and the limited detection efficiency have on the data, we include in the experimental $d\sigma/dQ$ spectrum (Fig. 2) also the predicted form of this spectrum, which is obtained when the parameterizations of Refs. 25 and 26 are used. The reduction of the measured cross section at large Q values, when compared to the prediction, is caused by the incomplete detection of fragments emitted at angles close to the grazing angle. This reduction is enhanced by the evaporation, which causes a shift of the "true" Q values into the direction of smaller values and simultaneously broadens the spectrum. Thus there is no one-to-one correspondence between "true" and measured Q values. Despite these shortcomings the binary analysis allows two conclusions to be made.

(i) The experimental setup has its maximum in detection efficiency for events with large energy loss. We are thus particularly sensitive to the strongly damped reactions.

(ii) For these reactions and the chosen bombarding energy, the studied systems behave similar to what has been observed elsewhere.[21] The elemental distributions are very broad and the deep-inelastic cross section does not vary with angle by more than a factor 10.

Although these conclusions are based on the binary analysis of the $m_f=1$ data, they remain valid when the data with larger fragment multiplicity are analyzed and when the proper evaporation corrections are included. These findings have established the guide lines for the Monte Carlo simulations of the deep-inelastic process. We have used the variety of exit channels that was experimentally found and we have used isotropic angular distributions. Obtaining a more precise input for the Monte Carlo simulations appears to be an almost unmanageable task since the properties of the primordial fragments before evaporation cannot be measured. Using the given input the Monte Carlo simulations reproduce the measured $d\sigma/dQ$, $d\sigma/dz$, and $d\sigma/d\theta_{c.m.}$ cross sections sufficiently well; in particular the shape of the $d\sigma/dQ$ spectrum is obtained as it was measured. Nevertheless, and as pointed out already, the quoted values of the total cross section must be considered correct only to the extent to which the total efficiencies thus obtained do not depend too strongly on this input.

B. The $m_f=2$ events

The $m_f=2$ events mainly have their origin in reactions where the exit channel contains two fragments and a number of light particles, but in 10–30 % of these events the correct number of fragments is larger than two and most probably three. The additional fragments were not detected by one of the ionization chambers; their presence, however, can be clearly deduced from several independent observations.

(i) A third fragment was detected by one of the parallel-plate avalanche detectors. This happens in 1–15 % of the $m_f=2$ events, depending on detector position. We will label these events as class-C events.

(ii) In the study of the $^{40}Ar + {}^{58}Ni$ reaction, the ionization chambers were positioned at angles sufficiently backward that a binary reaction, even when followed by light-particle evaporation, becomes undetectable. Still $m_f=2$

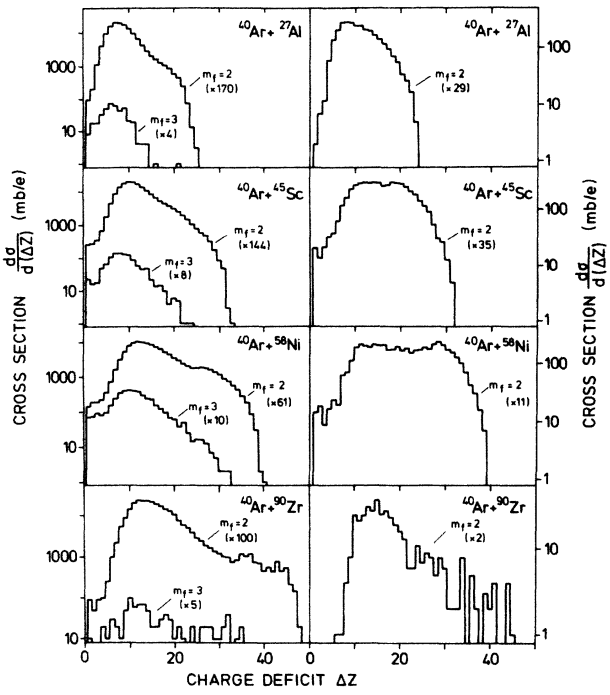

FIG. 3. The charge-deficit distributions for events with fragment multiplicites $m_f=2$ and $m_f=3$ are shown on the left-hand side. The charge-deficit distributions for $m_f=2$ events with a third fragment detected in the parallel-plate detectors are shown on the right-hand side.

events were observed at these detector settings. The large recoil momentum of a third fragment must have pushed the other two fragments into the directions which were covered by the detectors.

(iii) The charge deficit spectra of $m_f=2$ events (Fig. 3) extend to values too large to be ascribed to the evaporation of light particles. A simple estimate of the maximum ΔZ value allowed by evaporation is obtained if one assumes that the average separation energy of one neutron is 7 MeV and that of one proton is 9 MeV, and that charged and uncharged nucleons are evaporated with equal probability. One then gets, for the different targets, $\Delta Z_{max}=13$ (^{27}Al), 17 (^{45}Sc), 18 (^{58}Ni), and 21 (^{90}Zr). These values are about half of the maximum values measured, but they roughly coincide with the onset of the tails in the ΔZ spectra which can be recognized in Fig. 3. We conclude that these tails are entirely due to the three-fragment reactions. It should be pointed out that three-fragment reactions also contribute to events with charge deficits smaller than ΔZ_{max}. This can be clearly concluded from the charge-deficit spectra of class-C events also displayed in Fig. 3.

(iv) Events with only two fragments, i.e., true binary events, should be collinear, and thus the event plane is not defined. Subsequent light-particle evaporation destroys the collinearity. The additional momentum deficit $\Delta\mathbf{p}$, although small, facilitates the construction of the event plane, which is, for a statistical process with angular momentum $I=0$, randomly oriented with respect to the entrance-channel momentum. On the other hand, the momenta of three fragments have to be coplanar; the orientation of the event plane is determined by the reaction dynamics and only slightly modified by subsequent evaporation. Indeed, for small ΔZ values the measured event-plane orientation is close to $\langle\cos^2\alpha\rangle=0.33$, the value expected for a random orientation. With increasing ΔZ value, $\langle\cos^2\alpha\rangle$ decreases, indicating that the event plane becomes oriented almost perpendicular to the entrance channel momentum. This behavior is displayed in Fig. 4, which shows data from the $^{40}\text{Ar}+{}^{27}\text{Al}$ and $^{40}\text{Ar}+{}^{90}\text{Zr}$ reactions. Notice that we also find a decrease of $\langle\cos^2\alpha\rangle$ for very small ΔZ values and an increase for very large ΔZ values. This suggests the correlated emission of a few nucleons in the first case, perhaps caused by $I\neq0$. It also may point to the possibility that channels with four fragments contribute to events with very large ΔZ values.

Cases (i)—(iv) give unambiguous proof of the existence of channels with two and three fragments in all four reactions studied. Their separation in the $m_f=2$ data was achieved by making use of the properties already mentioned in cases (iii) and (iv): Reactions with only two fragments should be nearly collinear and the ΔZ values of these channels should not greatly exceed the values ΔZ_{max} listed in (iii). These criteria were implemented as elliptical cuts in the plane $d\sigma/d\Delta Z$ vs $d\sigma/d\sum\theta_{c.m.}$, where $\sum\theta_{c.m.}=\theta_{c.m.}(1)+\theta_{c.m.}(2)$, as shown in Fig. 5. We shall label events with two fragments class-A events, whereas all other $m_f=2$ events are class-B events. The relative strengths of class-A and class-B events were deduced from the count rates in these classes and the corresponding efficiency corrections obtained by means of the Monte Carlo simulation. The results are for four different targets: $P=0.14\pm0.05$ (^{27}Al), 0.14 ± 0.05 (^{45}Sc), 0.29 ± 0.04 (^{58}Ni), and 0.07 ± 0.05 (^{90}Zr), where

$$P=\sigma_{tot}(3\text{ fragm})/\sigma_{tot}(2\text{ fragm})\ .$$

The errors quoted are mainly due to the uncertainties in separating class-A from class-B reactions. In case of ^{90}Zr an additional error is caused by the carbon and oxygen contaminations of the target. Together with the measured cross section σ_{tot} in Table I, the ratios P may be used to calculate the two-fragment and three-fragment cross sections. The corresponding results are also listed in Table I.

It is evident that the class-A events are highly inelastic (for the class-B events, this shall be discussed in the next

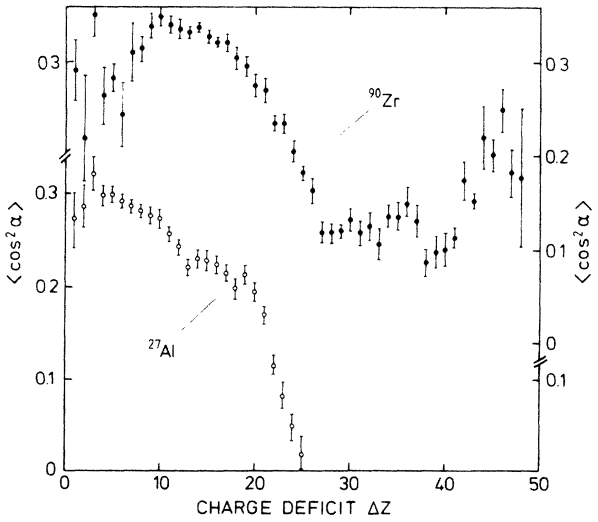

FIG. 4. The dependence of the event-plane orientation $\langle\cos^2\alpha\rangle$ on the charge deficit measured in the reactions $^{40}\text{Ar}+{}^{90}\text{Zr}$ and $^{40}\text{Ar}+{}^{27}\text{Al}$. Note the rupture in the scales for the two reactions.

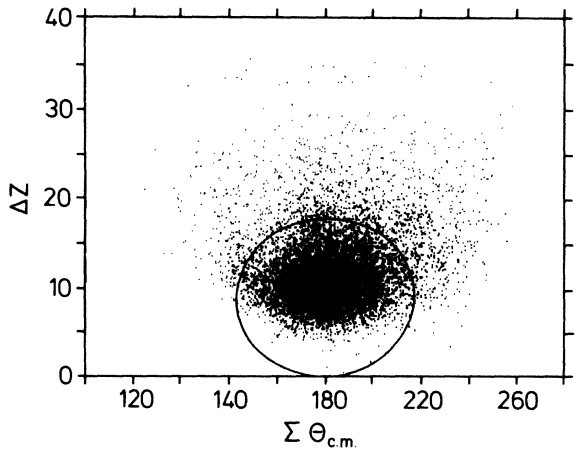

FIG. 5. Scatter plot of the extracted sum $\sum\theta_{c.m.}$ of the c.m. emission angles against the measured ΔZ values for $m_f=2$ events. The ellipse represents the cut used to separate class-A from class-B events (see text).

TABLE II. Measured mean values of the charge deficit and total kinetic energy loss for two-fragment and three-fragment reactions. The last three columns list the mean values of the breakup velocities in the rest system of the intermediate nucleus (i,j); see text. The first column contains the predicted maximum value of the total kinetic energy loss; see Refs. 25 and 26.

		Two-fragment		Three-fragment				
Target	$\lvert Q \rvert_{max}$ (MeV)	$\langle \Delta Z \rangle$	$\langle \lvert Q \rvert \rangle$ (MeV)	$\langle \Delta Z \rangle$	$\langle \lvert Q \rvert \rangle$ (MeV)	$\delta v(1,2)$	$\delta v(1,3)$	$\delta v(2,3)$
^{27}Al	209	$8.0^{+0.8}_{-0.3}$	180±15	6.5±0.3	160±15	1.17	1.20	1.15
^{45}Sc	270	$10.1^{+1.6}_{-0.4}$	235±20	8.7±0.3	215±20	1.09	1.10	1.12
^{58}Ni	293	$12.7^{+1.9}_{-0.4}$	280±25	10.7±0.4	245±25	1.13	1.18	1.28
^{90}Zr	333	$14.4^{+2.6}_{-0.5}$	330±30	13.0±0.6	295±30	0.92	1.10	1.09

section). Both the measured fragment energies and ΔZ values support this conclusion. The average ΔZ values for the four different targets are listed in Table II. Note that these values do not strongly depend on the detector positions. In case of the ^{40}Ar + ^{58}Ni reaction, where nine different position settings were measured, the variation in $\langle \Delta Z \rangle$ is not larger than ±3%. One may compare these values with the extrapolation from the low-energy data obtained in previous experiments.[22] This is done in Fig. 6. The error bars plotted represent the uncertainty in separating class-A from class-B events. The straight line corresponds to the relationship

$$\langle \Delta Z \rangle = \frac{1}{23.5}(E'_0 - 32) ,$$

which was found to represent all measured previous data within an uncertainty of $\delta \Delta Z = 0.5e$. At the present larger bombarding energy the average charge deficits are consistently smaller, but still seem to follow the slope of the extrapolated line. Also, the results for $m_f = 2$ events from the ^{58}Ni + ^{58}Ni reaction published in Ref. 9 follow this trend: the measured $\langle \Delta Z \rangle \approx 15.5$ is 10% smaller than the extrapolated value $\langle \Delta Z \rangle = 17.1$. From all these results it may be concluded that the average energy necessary to evaporate one charge is still 23.5 MeV, but that the conversion of the entrance-channel kinetic energy into excitation energy is less complete than that found at smaller bombarding energies. Considering the measured charge deficits, these values yield an estimate of the total kinetic energy loss $\lvert Q \rvert$ of the reaction. A similar estimate is obtained from the measured fragment energies E_i. Both agree for all targets within ±15 MeV. Note, however, that the values of $\lvert Q \rvert$ deduced from ΔZ and from E_i do not need to coincide, since the first is a measure of only the excitation energy, whereas the second also includes the ground-state masses. The derivation of the total kinetic energy loss is believed to be not accurate enough to justify the distinction between these two values. In Table II we have listed the deduced values of $\lvert Q \rvert$ and an upper limit for this quantity, which was obtained from the parametrizations of Refs. 25 and 26.

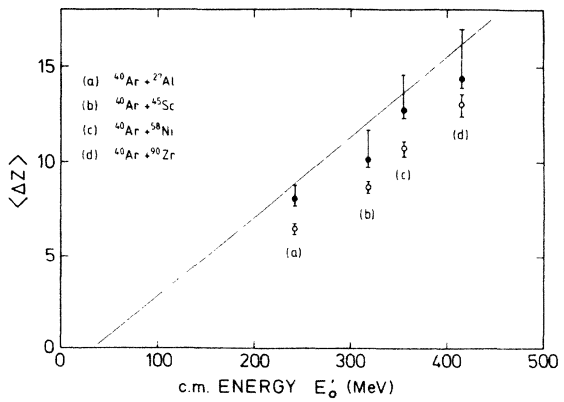

FIG. 6. The dependence of the average charge deficit on the c.m. energy for $m_f = 2$ events (dots) and $m_f = 3$ events (circles). The line displays the relation $\langle \Delta Z \rangle = 0.0426\ (E'_0 - 32)$ deduced in experiments with smaller bombarding energies (Ref. 8).

C. The $m_f = 3$ events

For the targets ^{27}Al, ^{45}Sc, and ^{58}Ni events with measured fragment multiplicity $m_f = 3$ were detected with a rate that was $(3-7) \times 10^{-3}$ smaller than the rate of $m_f = 2$ events. In case of the reaction with ^{90}Zr, the yield of $m_f = 3$ events was even smaller by a factor 5. This, however, is partly due to a reduced detection efficiency. Detection efficiencies were calculated by means of the Monte Carlo simulations and used to deduce the total three-fragment cross sections $\sigma_{tot}(3\ \text{fragm})$. The values obtained are in remarkable agreement with those listed in Table I.

In line with the discussions presented in the preceding subsection, it has to be checked whether or not $m_f = 3$ events also contain channels with four or more fragments. The dependence of the event-plane orientation on the charge deficit suggested that this might be the case. In addition, one of the parallel-plate avalanche detectors is triggered for $m_f = 3$ events with approximately the same relative rate that was found for $m_f = 2$ events. On the other hand, the ΔZ spectra depicted in Fig. 3 do not show an obvious extension to large ΔZ values. These arguments suggest that channels with four fragments do exist, but their relative strength is even smaller in comparison to the three-fragment reactions than was deduced in relating the three-fragment reactions to the two-fragment reactions. We estimate that less than 15% of the three-fragment cross section actually belongs to reactions with four fragments in the exit channel. This intensity is too small to allow these channels to be separated. We thus treat all measured $m_f = 3$ events as belonging to three-fragment reactions.

The mean value of the charge deficits of $m_f = 3$ events

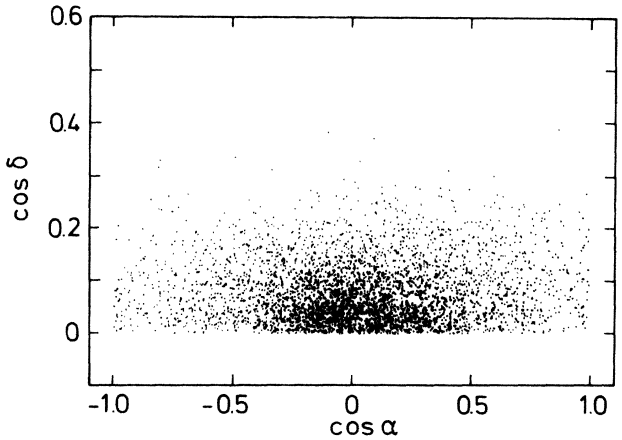

FIG. 7. Scatter plot showing the correlation between the planarity cosδ of the event plane and its orientation cosα for $m_f=3$ events in the $^{40}Ar + {}^{58}Ni$ reaction.

are always smaller than the corresponding values for $m_f=2$ events, as can be seen in Fig. 6 and Table II. On the average, the difference is $\langle \Delta Z \rangle_2 - \langle \Delta Z \rangle_3 = 1.6$. The relative independence of this difference on the center-of-mass energy suggests that for these events also the average energy required to emit one charge unit is 23.5 MeV. The mechanism responsible for the emission of light particles is also, in this case, most likely evaporation. However, because the $\langle \Delta Z \rangle$ values are smaller, the total kinetic energy loss $|Q|$ in the $m_f=3$ events is smaller also. Combining the information from the measured $\langle \Delta Z \rangle$ values and from the measured fragment kinetic energies, we have deduced estimates for the mean values of $|Q|$. These are listed in Table II. The differences between the kinetic energy losses for two-fragment and three-fragment reactions should be considered as the extra energies required to emit the third fragment. This energy slightly increases with the nuclear charge of the system.

The amount of $m_f=3$ events that have been accumulated in the present investigation makes it possible to perform a more detailed analysis of these events than could be done in the previous study.[8] Of particular interest are the properties of the event plane defined by the three fragment momenta and the momentum deficit, and the elemental and directional distributions of the three fragments when the data have been corrected for the light-particle evaporation.

As pointed out in Sec. II the properties of the event plane are described by two parameters: the planarity cosδ and the orientation cosα. As an example, the scatter plot Fig. 7 depicts the distributions of these two parameters for the reaction $^{40}Ar + {}^{58}Ni$. Apparently, in part of these data the parameters cosδ and cosα are correlated. The correlation requires that in the case where the event plane is well defined ($\cos\delta \approx 0$) the orientation of this plane is perpendicular to the entrance-channel momentum ($\cos\alpha \approx 0$). This implies that all momenta involved (fragment momentum, momentum deficit, beam momentum) are confined close to the event plane. The rest of the $m_f=3$ events are identified from the Monte Carlo simulations as being randomly distributed in the parameters cosδ and cosα. A conclusion as to why correlated and uncorrelated behavior is observed in the present investigations could not be reached. Both classes of $m_f=3$ events show almost identical results for all other parameters that were tested. Therefore, a further discrimination between them was considered not justified.

The results presented in the remaining part of this subsection have been corrected for light-particle evaporation as outlined in Sec. II. These results should thus describe the properties of the three fragments at an early step of the reaction, i.e., before light-particle evaporation sets in. Evaporation has a noticeable influence on the data, particularly for the very light systems. For example, in order to observe fragments with $Z>6$ after evaporation, the primary fragments, in general, have atomic numbers $Z>12$. Therefore the Dalitz plots of the elemental distributions shown in Fig. 8 for the reactions $^{40}Ar + {}^{27}Al$ and $^{40}Ar + {}^{58}Ni$, are depleted of events below a lower limit of Z. Above this limit the elemental distributions appear to be fairly isotropic with, perhaps, a small preference for the emission of one heavy and two light fragments. It should be noted that element distributions of similar isotropy were obtained from class-C events when these data are corrected by using $\langle \Delta Z(m_f=3) \rangle$ instead of $\Delta Z(m_f=3)$ in the correction factor α. We take this isotropy as clear evidence that complex-particle evaporation is not the reason for the occurrence of a third fragment. According to the $d\sigma/dZ=\sigma_0 Z^{-\tau}$ law, the evaporation process should give an enhancement of events with one light fragment. In order to illustrate this point the right-hand side of Fig. 8 displays the results from a Monte Carlo simulation of the $^{40}Ar + {}^{58}Ni$ reaction, where it is as-

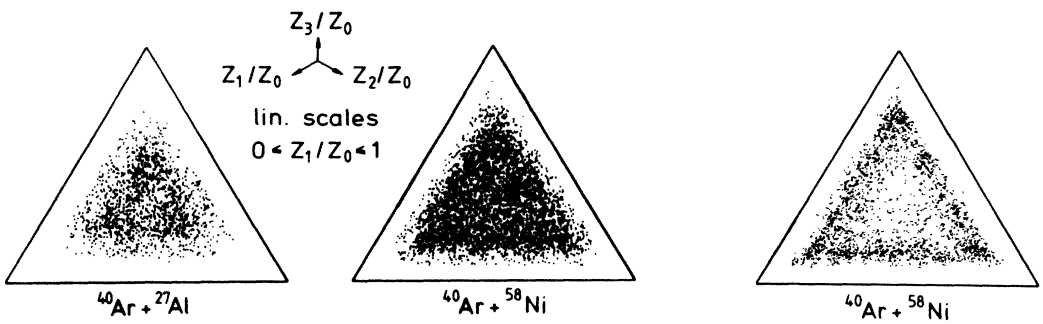

FIG. 8. Dalitz plots of the element distributions of $m_f=3$ events. The experimental data have been corrected for light-particle evaporation as discussed in the text (left). Monte Carlo simulation of $m_f=3$ events based on sequential evaporation with $d\sigma/dz \propto Z^{-3}$ (right).

sumed that a third fragment with $Z > 5$ is evaporated according to $d\sigma/dZ \propto Z^{-3}$. Further implications from this power-law dependence are discussed in Sec. IV. Note that in preparing the Dalitz plots we have taken a random ordering of Z_1, Z_2, Z_3 to account for the symmetry properties of the plots. In the usual convention the fragments are ordered with respect to their atomic number, i.e., $Z_1 \geqq Z_2 \geqq Z_3$.

The directional distribution of these fragments in the event plane is shown in Fig. 9. To obtain this figure data from all detector positions were used and normalized with respect to equal number of ^{40}Ar projectiles. Furthermore, the data were symmetrized with respect to the projectile momentum in order to further reduce the influence of the detector geometries. Still this influence can be recognized, particularly in case of the $^{40}\text{Ar} + {}^{58}\text{Ni}$ reaction, at certain angles in Fig. 9 where the yield is selectively large. Nevertheless, on the basis of the measured directional distributions, the measured elemental distributions and the fact that $m_f = 3$ reactions occur at almost mass-symmetric systems, the well-known breakup of the projectile coupled with incomplete momentum transfer can be ruled out as one possible fragmentation mechanism. This type of process is expected to occur at the present bombarding energy and, indeed, it is observed. However, it only occurs in $m_f = 2$ reactions with relatively small ΔZ values. In $m_f = 3$ reactions the measurements suggest that all three fragments are emitted with comparable momenta in random direction. As discussed in detail in Ref. 27, this implies that the breakup configuration is of the "closed" form. The question of whether this breakup is a prompt or a sequential process with a heavy nucleus of finite lifetime as an intermediate complex is still open. In the latter case the breakup process should have specific features[28] in the rest frame of the intermediate nucleus: The directional angular distribution of the two breakup fragments should be isotropic, and their velocities should be close to the velocities given by their mutual Coulomb interaction at the breakup point. Furthermore, these features should be independent of the recoil direction of the intermediate nucleus. Because of the problems with the detector geometries only the two last requirements were tested in detail.

The Coulomb velocities $v_C(i,j)$ were calculated using a Coulomb radius

$$R_C(i,j) = 1.4(M_i^{1/3} + M_j^{1/3}) \text{ fm} ,$$

where (i,j) is one of the three combinations of the indices 1,2,3 and $M_{i,j} = M_i + M_j$ is the atomic mass of the intermediate nucleus. This radius is believed to be a lower limit[28] and gives an upper limit for $v_C(i,j)$. In Fig. 10 the ratios of the measured to calculated velocities,

$$\delta v(i,j) = v_{\text{rel}}(i,j)/v_C(i,j) ,$$

for the reactions $^{40}\text{Ar} + {}^{58}\text{Ni}$ and $^{40}\text{Ar} + {}^{90}\text{Zr}$ are shown; Table II presents the mean values of this parameter for all

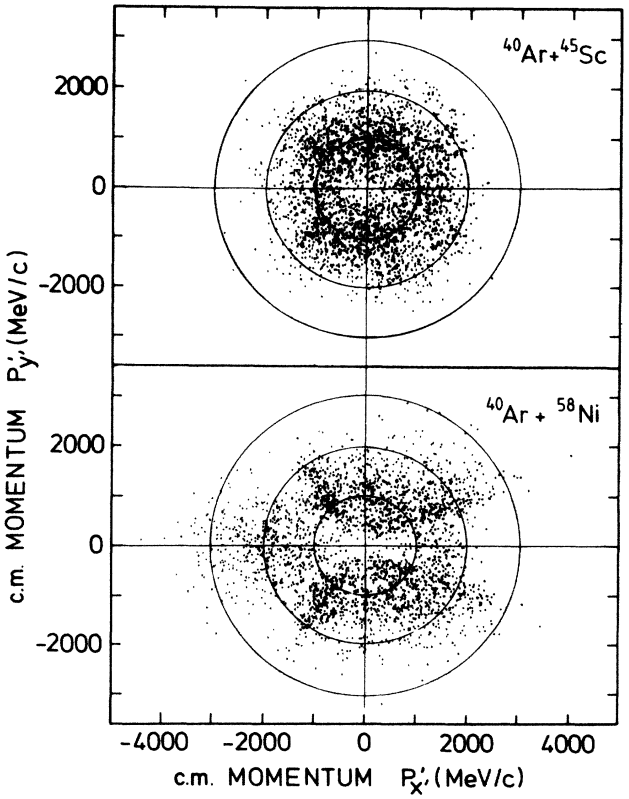

FIG. 9. Directional distributions of three fragments in the event plane. The data have been corrected for light-particle evaporation as discussed in the text.

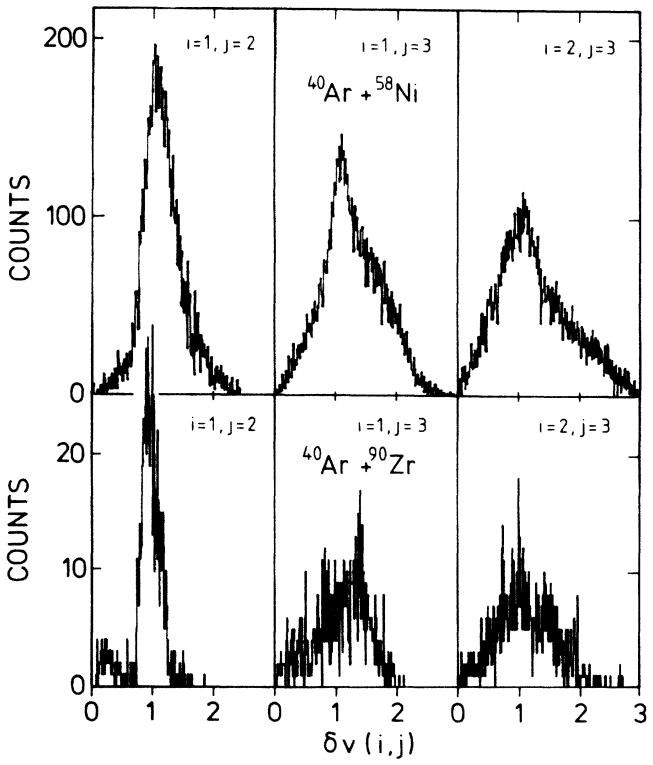

FIG. 10. Relative velocities $\delta v(i,j)$ of fragments i,j in the rest system of the intermediate nucleus with charge $Z_i + Z_j$. The relative velocities are presented as ratios $\delta v(i,j)$ with the expected Coulomb velocities $v_C(i,j)$; see text.

reactions studied. In general, the distributions of the relative velocities are rather broad and the mean values are systematically larger than calculated, except for one case in the $^{40}Ar + {}^{90}Zr$ reaction. Particularly instructive is the $^{40}Ar + {}^{58}Ni$ reaction, where $\delta v(i,j)$ increases with decreasing mass of the intermediate nucleus or increasing mass of the spectator nucleus. This is expected when the lifetime of the intermediate nucleus is short enough that the nuclear charge of the spectator causes an observable distortion of the velocities of the breakup fragments. Only in case of $^{40}Ar + {}^{90}Zr$ reaction is the mean value of $v_{rel}(1,2)$ smaller than calculated. Furthermore, 74% of the $m_f=3$ data from this reaction can be selected that have a narrow distribution of $v_{rel}(1,2)$. This selected data sample is displayed in Fig. 10. It is concluded that at least part of the data from the $^{40}Ar + {}^{90}Zr$ reaction is in agreement with the preposition that a light spectator and a heavy intermediate nucleus are formed in the first step of the reaction. Subsequently, the latter fissions into two heavy fragments.

IV. DISCUSSION

At the present bombarding energy of 15 MeV/u, we have found in all reactions studied (i.e., $^{40}Ar + {}^{27}Al$, ^{45}Sc, ^{58}Ni, ^{90}Zr) sizable contributions from reactions with three heavy fragments in the exit channel. These contributions are strongest ($P=0.29$) in the reaction with the ^{58}Ni target and weakest ($P=0.07$) in the reaction with the almost twice as heavy ^{90}Zr target. Compared to similar studies with ^{35}Cl projectiles at 11 MeV/u bombarding energy,[8] the P factors have increased by more than a factor 2. Similar studies were also reported for the $^{58}Ni + {}^{58}Ni$ system at 15.3 MeV/u bombarding energy ($P=0.02$) (Ref. 9) and the $^{128}Xe + {}^{122}Sn$ system at 12.5 MeV/u bombarding energy ($P=0.12$) (Ref. 7). These factors apply for reactions with large energy losses and therefore correspond to the situation encountered in the present study. All these data suggest that the probability for three-fragment reactions is largest in asymmetric systems with a total mass of $M \approx 100$. It is probably also true that the mechanism responsible for the occurrence of three fragments is not unique in all systems studied. In the heavier systems of Refs. 6 and 7 it was suggested that sequential fission is the dominant process. In the present investigation at least part of the data from the $^{40}Ar + {}^{90}Zr$ reaction also fit into such an interpretation. On the other hand, it is not believed that this mechanism could also be responsible for the three-fragment channels found in the $^{40}Ar + {}^{27}Al$ reaction. A simple estimate based on the liquid-drop fission barrier[28] shows that the fission probability should be less than $P_f=10^{-3}$ for such light systems and angular momenta $l<20$ whereas $P_f=0.07$ could occur for an intermediate nucleus of mass $A=90$ and $l\approx 40$ under the present conditions.

An alternative mechanism, but still of statistical origin, could be the complex-particle evaporation from one of the primary heavy fragments. Theoretical predictions based on such a model have been reported in Refs. 4, 10, and 13 and compared to experimental data. It is believed that evaporation should lead to an element distribution of the

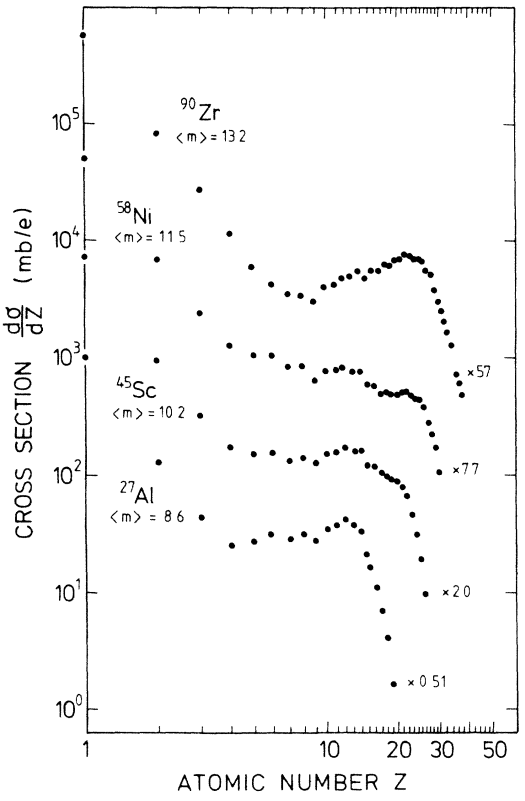

FIG. 11. Deduced elemental cross sections for the four reactions studied. This figure also gives the total associated fragment and particle multiplicity $\langle m \rangle$.

form $d\sigma/dz=\sigma_0 Z^{-\tau}$, where τ is a function of the nuclear temperature. With the present temperatures of $T=4.5$ MeV, one expects $\tau \approx 3$. It is the characteristic feature of the present experimental technique that the light particles due to evaporation were not individually identified, but were combined to yield the total light-particle charge, etc. In order to compare our measured element distributions with the predictions, we have to assume that the power law holds for the light-mass component of the evaporation process. The element distributions deduced with this assumption are depicted in Fig. 11. Also shown are the mean values $\langle m \rangle$ of the total multiplicity deduced from such an interpretation. Obviously, the particle yield follows the expected power law only up to the nuclear charge $Z=4$, with perhaps a small extension to larger charges in the case of the $^{40}Ar + {}^{90}Zr$ reaction. This is not surprising since it was assumed to be correct for such light particles. For the heavier particles, however, the measured strong yield certainly does not follow the evaporation prediction. Of course, this conclusion only corroborates the findings already presented in Sec. III C.

There are, indeed, several indications that the mechanism responsible for the emission of three fragments is not of pure statistical origin. From our analysis of their linear momenta it was concluded that they are emitted from a specific breakup configuration which was called "closed" in accordance with the discussion of Ref. 27.

The term "closed" describes an oblate configuration.[29] The complementary prolate configuration does not seem to have been formed with observable yield in the present reactions, although it has a much larger detection probability with our experimental technique. Furthermore, both the analysis of the $m_f=2$ and 3 events indicate that a large fraction of the three fragments are emitted into a plane whose normal vector is perpendicular to the entrance-channel momentum. Since this is the only way in which the normal direction may coincide with the direction of the entrance-channel angular momentum, it is concluded that angular momentum effects are of major importance in the breakup mechanism. In Table I we have listed the range of entrance-channel angular momenta as deduced from the measured cross sections by using the sharp cutoff prescription. From the parametrizations of Refs. 25 and 26, it is expected that all four reactions have sizable fusion cross sections. It is assumed that the angular momentum values responsible for the breakup process are within $l_{cr} < l < l_{max}$ and probably are close to l_{max} since the breakup process has a lower energy threshold at approximately 10 MeV/u.

The behavior of nuclear systems of oblate shape and with large angular momenta was studied in detail by Wong.[30,31] For sufficiently large angular momenta, the system can develop into a toroidal shape because this causes the rotational and Coulomb energies to decrease, whereas the surface energy increases. In our systems the minimum energies are reached for aspect radii $R/d \approx 2-2.5$, where R is the major radius of the torus and d is the minor radius of the torus.[31] Such a system, however, is generally unstable and can decay into any number λ of fragments with $\lambda \geqq 2$. Of particular interest for our studies are the decay probabilities for $\lambda=2,3$, which become larger than zero when the stiffness constants K_λ become negative. Wong[19] has calculated the constants K_λ for our systems assuming a rigid-body rotation. The results are plotted in Fig. 12. According to the decay criterium the tori are unstable against breakup into two fragments in all systems. The breakup into three fragments should not occur for the $^{40}Ar + {}^{27}Al$ system. The observation of three fragments in this system also remains unexplained by these calculations. This is not considered a proof that excludes the possibility for toroidal shapes in nuclear systems with large rotational energy. The experimental search for such systems has just started and the model may be too simplified for such detailed predictions. Otherwise, it encompasses several of the observations made in this study: the formation of systems with high angular momentum, the dominance of oblate breakup configurations, and two- and three-fragment emission into the event plane that seems to be uncorrelated with the beam momentum.

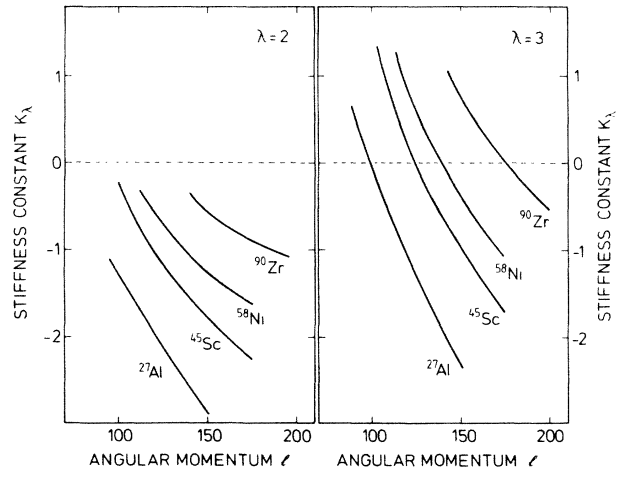

FIG. 12. The dependence of the stiffness constant K_λ on the angular momentum l of a nuclear torus in rigid rotation. The total mass and charge of the torus is obtained by adding $M=40$, $Z=18$ to the mass and charge of the target elements used in this figure to characterize different systems.

V. SUMMARY AND CONCLUSIONS

In the present investigations we have studied ^{40}Ar induced reactions on four different targets (^{27}Al, ^{45}Sc, ^{58}Ni, ^{90}Zr) at 15 MeV/u bombarding energy. The main interest was in the identification of reactions with at least three heavy fragments in the exit channel. In all four reactions such channels were observed at large kinetic energy losses. Compared to the binary, strongly damped collisions, their relative strengths are on the order of 7–14 % for the light ($^{40}Ar + {}^{27}Al$, ^{45}Sc) and heavy ($^{40}Ar + {}^{90}Zr$) systems, but amounts to 23% for the $^{40}Ar + {}^{58}Ni$ system. A more detailed dependence of the fragmentation process on energy loss could not be deduced since fragmentation is accompanied by strong light-particle evaporation, which severely effects the kinematic properties of the fragments in the studied systems.

The total charge of the light evaporation products in two- and three-fragment channel increases linearily with the c.m. bombarding energy. The rate of increase suggests that an energy of 23.5 MeV is needed to evaporate one charge unit. This should be considered as twice the energy to evaporate one mass unit. The amount of charge lost by evaporation is smaller in the three-fragment channels than in the two-fragment channels; still it accounts, under the present conditions, for at least 20% of the total nuclear charge of the systems. The proposition that one of the fragments in the three-fragment channels is due to evaporation also is not supported by the reconstructed element distributions. These distributions do not show the expected increase of yield with decreasing charge of one fragment, but are rather isotropic in their charges of all three fragments. Also, a fission process is most likely not the source for the respective subset of fragments, except in case of the $^{40}Ar + {}^{90}Zr$ reaction, where part of the data is in agreement with such an interpretation. At the moment the model of a hot and fast rotating reaction composite which disintegrates into three fragments appears to give the most concise description of our results. The question of whether or not part of the binary reactions also actually comes from such a process is open and difficult to answer since these channels have a much stronger overlap

with the entrance channel.

The experiments also suggest that channels with even larger numbers of fragments exists. Their contribution is still weak, but can be expected to increase with bombarding energy, judging from the behavior of the three-fragment channels. This and the increasing strength of evaporation introduce severe experimental problems. The solution to these problems can probably only come from a detector with better 4π coverage and larger granularity, capable of measuring all kinematic variables of the detected reaction products.

ACKNOWLEDGMENTS

We are grateful to C. Y. Wong, who performed, for the studied reactions, the calculations based on the rotating nuclear toroid. Part of this work was supported by the Bundesministerium für Forschung and Technologie.

[1]M. Fatyga, K. Kwiatkowski, V. E. Viola, C. B. Chitwood, D. J. Fields, C. K. Gelbke, W. G. Lynch, J. Pochodzalla, M. B. Tsang, and M. Blann, Phys. Rev. Lett. **55**, 1376 (1985).

[2]R. Trockel, K. D. Hildenbrand, U. Lynen, W. F. J. Müller, H. J. Rabe, H. Sann, H. Stelzer, R. Wada, N. Brummund, R. Glasow, K. H. Kampert, R. Sauter, D. Pelte, J. Pochodzalla, and E. Eckert, Gesellschaft für Schwerionenforschung Report No. GSI-85-45, 1985 (unpublished).

[3]D. J. Fields, W. G. Lynch, C. B. Chitwood, C. K. Gelbke, M. B. Tsang, H. Utsunomiya, and J. Aichilin, Phys. Rev. C **30**, 1912 (1984).

[4]L. G. Sobotka, M. A. McMahan, R. J. McDonald, C. Signarbieux, G. J. Wozniak, M. L. Padgett, J. H. Gu, Z. H. Liu, Z. Q. Yao, and L. G. Moretto, Phys. Rev. Lett. **53**, 2004 (1984).

[5]A. I. Warmick, H. H. Wiemann, H. H. Gutbrod, M. R. Maier, J. Peter, H. G. Ritter, H. Stelzer, F. Weik, M. Freedmann, D. J. Henderson, S. B. Kaufmann, E. P. Steinberg, and B. D. Wilkins, Phys. Rev. C **27**, 1083 (1984).

[6]D. V. Harrach, P. Glässel, Y. Civelekoglu, R. Manner, and H. J. Specht, Phys. Rev. Lett. **42**, 1728 (1979).

[7]P. Glässel, D. V. Harrach, H. J. Specht, and L. Grodzins, Z. Phys. A **310**, 189 (1983).

[8]D. Pelte, U. Winkler, J. Pochodzalla, M. Bühler, A. Gorks, and B. Weissmann, Nucl. Phys. **A438**, 582 (1985).

[9]T. C. Awes, R. L. Ferguson, R. Novotny, F. E. Obenshain, F. Plasil, V. Rauch, G. R. Young, and H. Sann, Phys. Rev. Lett. **55**, 1062 (1985).

[10]W. A. Friedmann and W. G. Lynch, Phys. Rev. C **28**, 16 (1983).

[11]A. D. Panagiotou, M. W. Curtain, H. Toki, D. K. Scott, and P. J. Siemens, Phys. Rev. Lett. **52**, 496 (1984).

[12]H. Machner, Phys. Rev. C **31**, 1271 (1985).

[13]D. H. E. Gross, Hahn-Meitner Institut Report No. HMI-P-84/17 TH, 1984 (unpublished).

[14]W. Bauer, D. R. Dean, U. Mosel, and U. Post, Phys. Lett. **150B**, 53 (1985).

[15]J. Aichilin and J. Hufner, Phys. Lett. **136B**, 15 (1984).

[16]A. S. Goldhaber, Phys. Lett. **51B**, 306 (1974).

[17]J. Knoll and B. Strack, Phys. Lett. **149B**, 45 (1984).

[18]J. Bondorf, R. Donangelo, I. N. Mishuotin, and H. Schulz, Nucl. Phys. **A444**, 460 (1985).

[19]C. Y. Wong, Phys. Rev. C **30**, 1949 (1984).

[20]D. Jacquet, E. Dueck, J. M. Alexander, B. Borderie, J. Galin, D. Gardes, D. Guerreau, M. Lefort, F. Monnet, M. F. Rivet, and X. Tarrago, Phys. Rev. Lett. **53**, 2226 (1984).

[21]S. Gralla, R. Bock, A. Gobbi, K. D. Hildenbrand, J. Kuzminski, U. Lynen, W. F. J. Müller, A. Olmi, M. Petrovici, H. Sann, H. Stelzer, J. Toke, and H. J. Wollersheim, Gesellschaft für Schwerionenforschung Report No. GSI-84-36, 1984 (unpublished); S. Gralla, Ph.D. thesis, University of Heidelberg, 1985 (unpublished).

[22]J. Betz, H. Graf, R. Novotny, D. Pelte, and U. Winkler, Nucl. Phys. **A408**, 150 (1983).

[23]U. Winkler, B. Weissman, M. Bühler, A. Gorks, R. Novotny, and D. Pelte, Nucl. Phys. **A425**, 573 (1984).

[24]U. Lynen, H. Stelzer, A. Gobbi, H. Sann, and A. Olmi, Nucl. Instrum. and Methods **163**, 141 (1979).

[25]H. J. Wollersheim, Gesellschaft für Schwerionenforschung Report No. GSI-84-34, 1984 (unpublished).

[26]W. W. Wilcke, J. R. Birkelund, H. J. Wollersheim, A. D. Hoover, J. R. Huizenga, W. U. Schröder, and L. E. Tubbs, At. Data Nucl. Data Tables **25**, 389 (1980).

[27]D. Pelte and U. Winkler, Nucl. Phys. **A243**, 164 (1984).

[28]R. Vandenbosch and J. R. Huizenga, *Nuclear Fission* (Academic, New York, 1973).

[29]J. A. Marhun and W. A. Greiner, in *Heavy Ion Collisions*, edited by R. Bock (North-Holland, Amsterdam, 1980), Vol. 2, p. 397.

[30]C. Y. Wong, Phys. Rev. C **17**, 331 (1978).

[31]C. Y. Wong, Ann. Phys. (N.Y.) **77**, 279 (1973).